7th International Symposium on Superalloy 718 and Derivatives
Edited by: E.A. Ott, J.R. Groh, A. Banik, I. Dempster, T.P. Gabb, R. Helmink, X. Liu, A. Mitchell, G.P. Sjöberg, and A. Wusatowska-Sarnek
TMS (The Minerals, Metals & Materials Society), 2010

MICROSTRUCTURE EVOLUTION IN THE NICKEL BASE SUPERALLOY ALLVAC®718PLUS™

K. Löhnert[1], F. Pyczak[2]

[1]Rolls-Royce Deutschland Ltd&Co KG, Eschenweg 11,
15827 Blankenfelde-Mahlow, Germany
[2]GKSS Research Centre Geesthacht GmbH, Max-Planck-Straße 1,
21502 Geesthacht, Germany

Keywords: 718Plus, Gamma-Prime, Delta, TEM

Abstract

Nickel base superalloys experience significant changes of the microstructure during processing as well as in service. The mechanical properties are predominantly determined by microstructure parameters like grain size, γ′-precipitate diameter and volume fraction, etc. Thus, knowledge about the microstructure evolution during processing is a necessary prerequisite to employ novel alloys as Allvac®718Plus™ in service.

In the present study, microstructure evolution during heat treatment in particular has been investigated. Electron microscopy and especially transmission electron microscopy (TEM) have been used to characterise the microstructure changes in Allvac®718Plus™. The two major phases were found to be γ′- and δ-phase. By analysing selected area diffraction patterns from a large number of particles, it could be shown that nearly no γ′′-phase is present in Allvac®718Plus™. Emphasis was put on the development of γ′- and δ- phase during typical heat treatment steps performed during processing. Here particle growth, the volume fractions of the phases as well as their crystallographic relationship and chemical composition were monitored using imaging, diffraction and energy dispersive spectroscopy in TEM. The interfaces between the δ- and surrounding γ/γ′-phase were investigated using high resolution TEM. They are flat and parallel to the {111} plane of γ/γ′-phase and the (010) plane of δ-phase.

Introduction

Allvac®718Plus™ (hereafter 718Plus) is a newly developed Nickel base superalloy that combines the good processability and weldabilty of Inconel 718 (hereafter 718) with the high temperature capability of Waspaloy. It is therefore suitable for use as static parts in jet engines such as turbine or combustor cases and is also a promising candidate for turbine disc applications. Overview articles describing development and properties of 718Plus can be found in Reference [1]. Essentially, due to changes in chemical composition (see **Table 1**) in comparison to 718, 718Plus is strengthened by the ordered $L1_2$ γ' phase. This is mainly accomplished by changing the Al and Ti content and ratio. Nb increases the strength and decreases the precipitation rate of γ' phase [2]. By adjusting Co, W and Fe contents, solid solution strengthening and thermal stability were improved.

Table 1: Comparison of chemical composition of 718Plus and 718 (in wt%).

	Ni	Cr	Mo	W	Co	Fe	Nb	Ti	Al	C	P	B
718Plus	Bal.	18,0	2,8	1,1	9,0	9,0	5,5	0,7	1,5	0,025	0,012	0,006
718	Bal.	18,1	2,9	---	---	18,0	5,4	1,0	0,5	0,025	0,007	0,004

The formation of γ' phase makes 718Plus useable at temperatures up to 704°C. This is equivalent to a 55°C temperature advantage over 718, which is strengthened by the metastable DO_{22} bct γ'' phase. To strengthen the grain boundaries in 718Plus, grain boundary δ phase can be precipitated during heat treatment. An adequate amount of δ on the grain boundaries can improve mechanical properties such as high-temperature ductility or crack propagation resistance [3].
With respect to microstructure and mechanical properties, 718Plus has so far been optimised for application in static engine parts, with the main focus on tensile and stress rupture properties [4]. To make it available for rotating turbine components, the microstructure needs to be optimised for a best possible balance of crack propagation resistance and creep strength as well as high LCF strength. Therefore, a thorough understanding of microstructure development during a complex post forging heat treatment cycle is required. It is the aim of this study to identify the main phases present in 718Plus and to establish which microstructure parameters are most affected by certain steps of the overall heat treatment. From this it can be concluded, which heat treatment steps are decisive to produce the desired microstructure for optimum alloy performance in service.

Experimental

The chemical composition of the material used in this study has already been given in Table 1. JMatPro software along with the TTNi7 database was used to calculate regions of phase stability in 718Plus [5]. Non-equilibrium behaviour of 718Plus was studied using a Netzsch STA 404 Differential Scanning Calorimetry (DSC) apparatus.
From as-forged disc grade material with a homogeneous grain size of ASTM 10-11, cube shaped specimens with an edge length of 5 mm were wire-cut. The specimens were subsequently subjected to different heat treatments in order to study the precipitation sequence of phases present in 718Plus. First, pre-solution treatments at temperatures between 840 °C and 870 °C were applied for varying durations to investigate δ-phase precipitation at the grain boundaries. After pre-solution heat treatment, the specimens were further solution annealed, followed by an ageing cycle. The ageing cycle was carried out in two variations – single step at 788 °C and standard two step at 788 °C and 704 °C, respectively. The duration of the first ageing cycle was varied between 2 and 12 hrs, the second one was kept constant at 8 hrs. At different stages of the heat treatment process, TEM specimens were prepared. The as-heat treated specimens were ground to a thickness in the range of 100 µm and twin jet electropolished using a solution of perchloric and acetic acid. TEM micrographs and energy dispersive X-ray (EDX) measurements were performed using a Philips CM200 with an Oxford EDX system while high resolution TEM investigations were done at a FEI TITAN 80-300 with C_s-correction.

Results and Discussion

JMatPro phase stability predictions

For thermodynamic equilibrium, JMatPro predicts the presence of δ and γ′ phases, as shown in Figure 1. The predicted solvus temperature of δ-phase is 1026 °C, which is higher than that of γ′ at 976 °C. Both values are however lower than the modeling results obtained by Cao et al. with the same software tool, where 1065 °C were predicted as δ-solvus and 995 °C as γ′-solvus, respectively [6]. Therefore, and to clarify non-equilibrium behaviour, DSC measurements on as-forged material were carried out. There, a δ-solvus of 998 °C and a γ′-solvus of 960 °C have been determined. These results could be confirmed by extensive microstructural analyses (SEM, TEM) following industrial forging and heat treatment trials, which are not reported herein. They also agree well with DSC results reported by other authors [7]. At 650 °C, JMatPro calculates a phase fraction of 19,5 wt% γ' and 9,0 wt% δ, respectively.

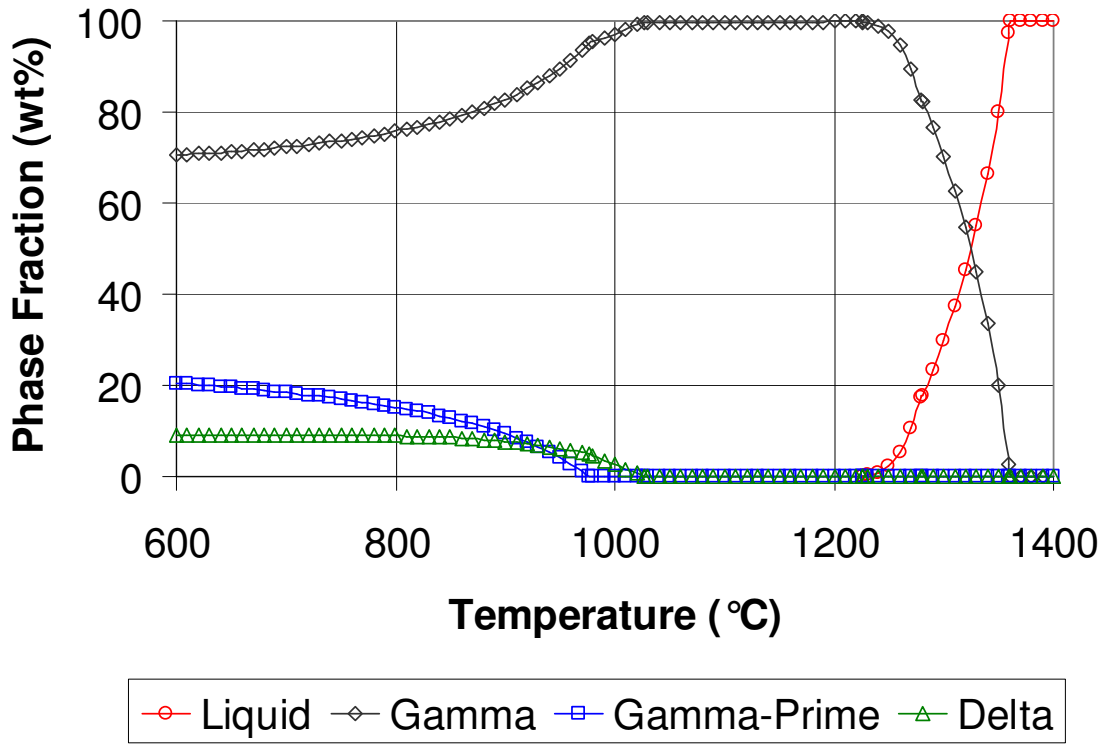

Figure 1: Phase fractions of γ, γ′ and δ phases in wt% over temperature, as predicted by JMatPro.

Apart from the main δ and γ′ phases, JMatpro also predicts the presence of a Nb rich MC-carbide and a Mo-rich MB_2-boride. At 650 °C, the phase fractions are very low with 0,2 wt% for MC and 0,02 wt% for MB_2. They are not shown in Figure 1.

Based on the data obtained by modelling and DSC, the development of γ′ and δ precipitates during heat treatment was studied.

Development of γ'-phase during heat treatment

It is well established that size, morphology, distribution and composition of γ' phase play a key role for the mechanical properties of Nickel base superalloys. Figure 2 shows the development of γ' precipitates at typical stages of heat treatment. It is obvious, that, at all stages, the size distribution of the γ'-phase is monomodal. A size distribution of primary, secondary and tertiary γ', which is known from other polycrystalline Ni base superalloys such as RR1000 [8], was not observed under the heat treatment conditions under investigation here.

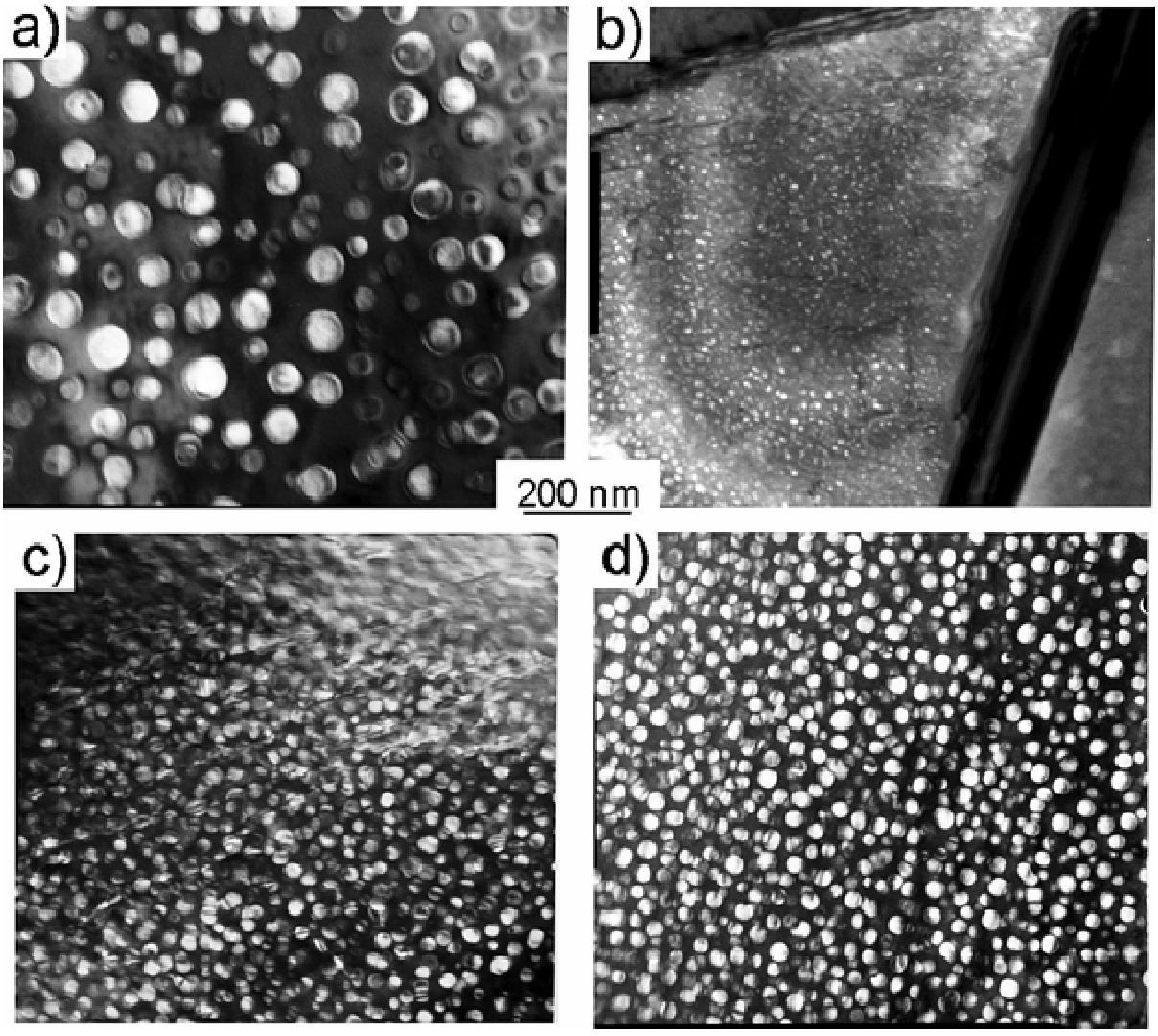

Figure 2: γ' microstructure in specimens representing different typical stages of the heat treatment procedure pictured as TEM dark field micrographs using the superlattice <001> reflection: a) γ' after pre-solution heat treatment, b) γ' after solution heat treatment, c) γ' after single step age, d) γ' after two step age.

As the pre-solution treatment is carried out well below γ'-solvus, the coarse primary γ' which develops during cooling from forging temperature is still present (Figure 2a). It has an average size of 90 nm to 100 nm. During solution treatment, the coarse primary γ' is dissolved and is re-precipitated out of a supersaturated solid solution during cooling from solution temperature

(Figure 2b). The ageing treatment aims at coarsening and stabilizing the γ' population. Annealing at 788 °C coarsens the γ'-particle diameter (Figure 2c). This particle diameter does not change significantly when a second ageing step at 704 °C is added (Figure 2d). This shows that γ' coarsening is rather slow. It has been suggested previously, that the slow coarsening kinetics can be attributed to the low diffusion coefficient of Nb, which partitions to γ' [6,9].
The coarsening of γ' was investigated for ageing times of the first ageing step between 2 and 12 hrs. The results are plotted in Figure 3, which shows, that the γ' sizes are very similar regardless whether a single or two step age has been applied. Thus, with respect to γ' size, a single step age can generate similar microstructures as the more complex two step ageing procedure.

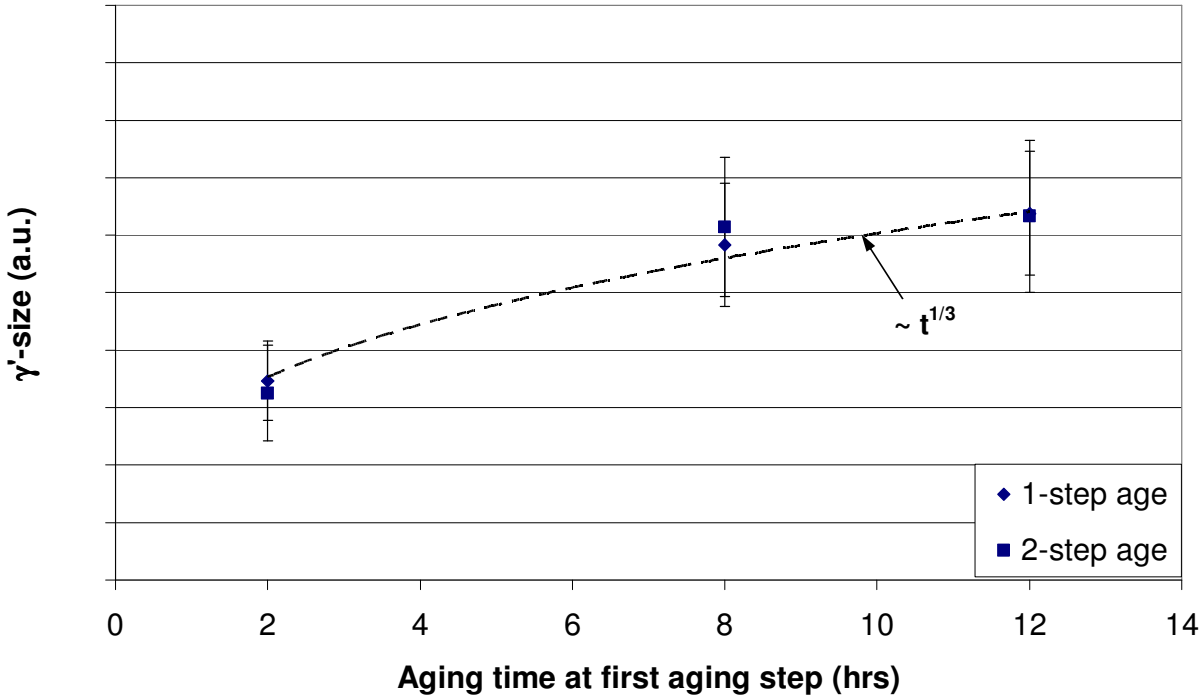

Figure 3: γ' particle size plotted over annealing time at 788 °C.

It can also be inferred from Figure 3, that the increase in γ'-particle diameter follows a Lifshitz-Slyozov-Wagner type relationship, i.e. is proportional to $t^{1/3}$. This relationship is also valid for longer ageing times and higher ageing temperatures, as was recently shown by Zickler et al. [10].

The detailed composition and volume fraction of γ' in fully heat treated material have not been determined yet. Both will therefore be studied next.

Composition and volume fraction of γ'-phase

The composition of γ' was determined by TEM-EDX. For comparison, the γ matrix composition was determined as well. For this purpose, ten measurements of the matrix phase and ten measurements in γ'-particles in a fully heat treated specimen, i.e. after two step ageing, were performed. Due to drift of the illuminated region, the small size of the γ'-precipitates and the

narrow γ-matrix channels, some measurements had to be discarded because the detection volume had drifted from the γ- to the γ′-phase or vice versa during the measurement. As a criterion to sort out measurements which could not be attributed unambiguously to either the γ- or the γ′-phase all measurements with Cr contents between 11 and 24 at.% were discarded. Cr is an alloying element which is known to partition predominantly to the γ-matrix phase. Accordingly, it was assumed that all measurements with intermediate Cr contents do not represent situations where the detection volume was either fully in the γ- or γ′-phase.
Table 2 shows the chemical composition of the phases γ and γ′. The γ′-precipitates are enriched with alloying elements such as Al, Ti, and Nb which are known to be typical γ′-forming elements [11], while Cr, Fe, Co and Mo mainly partition to the γ-matrix.

Table 2: Composition of γ and γ′ phases in 718Plus (at%).

Element	**Al**	**Ti**	**Cr**	**Fe**	**Co**	**Ni**	**Nb**	**Mo**	**W**
γ-(matrix)	2,02	0,03	26,6	11,4	9,25	45,8	3,40	1,72	(-0,18)
γ′ phase	13,8	1,88	10,1	4,97	5,39	54,9	6,94	0,92	1,07

It is also possible to determine the mole fraction of the γ′-precipitate phase from the chemical composition of the phases γ and γ′ and the overall alloy composition. The method employed here is known as the Blavette method or lever rule [12]. This method is useful as the reliable determination of the γ′-volume fraction from TEM- or SEM-micrographs is difficult due to the small size of the γ′-particles in 718Plus. To apply the lever rule, the difference between the concentration of an alloying element in the γ matrix and the nominal alloy composition (c^{γ}-c^{0}) is plotted versus the difference of the concentration of an alloying element in the γ and γ′ phases (c^{γ}-$c^{\gamma'}$). This is repeated for the different alloying elements. The slope of this plot is equivalent to the mole fraction of the γ′-phase according to the lever rule. Due to the fact that the 718Plus alloy under investigation is not two phase γ / γ′, but also contains δ-phase it is not possible to use the nominal alloy composition as c^{0} in the formula for the lever rule plot because a certain amount of alloying elements is present in the δ-phase. Therefore, the mean concentration c^{0} was derived from an area scan EDX measurement over a specimen position where no δ-particles or other third-phase particles were present. Figure 4 shows the lever rule data for the investigated 718Plus specimen.

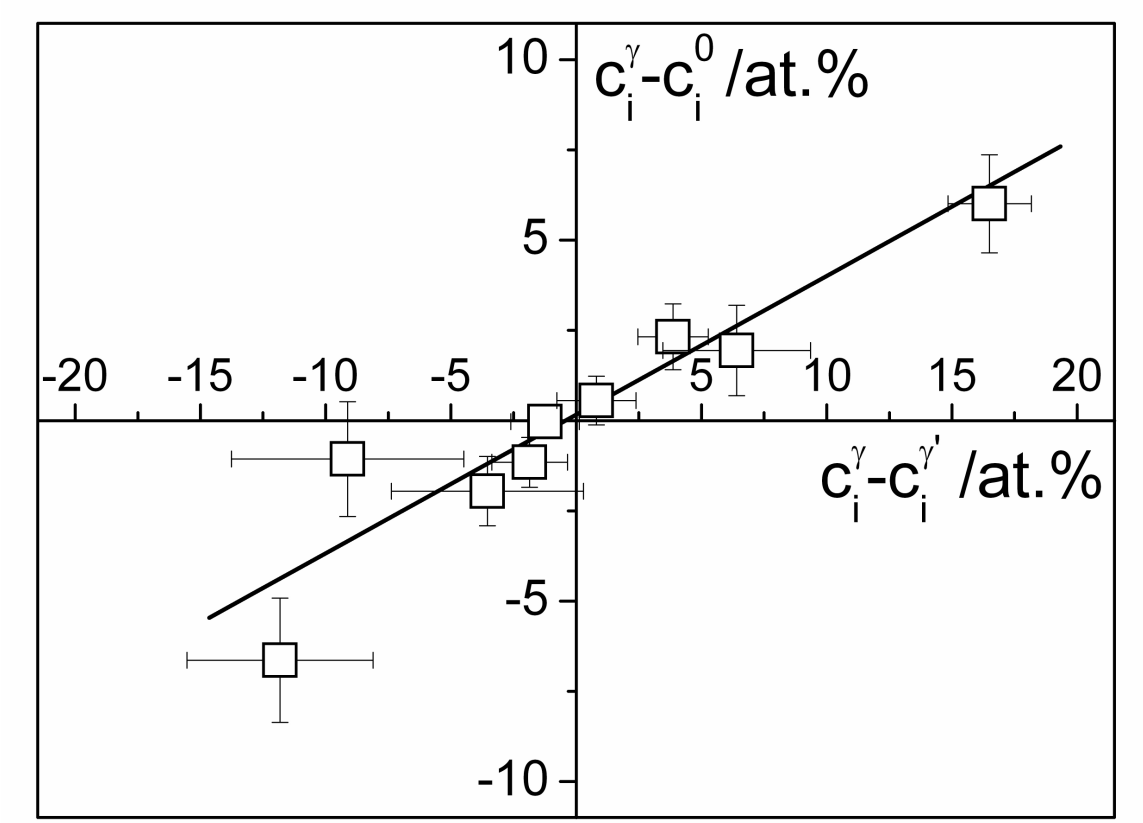

Figure 4: Blavette plot of element concentrations in the γ phase, γ′ phase and the mean alloy composition. The slope represents the mole fraction of γ′ particles, which is 38 %. After correction for δ-phase, the mole fraction is 36,8 %.

From the slope of the graph, a mole fraction of 38 % for the γ′-phase is found. However, this γ′ fraction must be corrected for the amount of δ-phase present in the investigated specimen. The volume fraction of the latter was determined to be 3,2 % using image analysis of an appropriate number of respective SEM micrographs. Also, in order to compare the experimental γ′ fraction to the JMatPro predictions, it was converted to wt%. The correction for δ-phase fraction and conversion resulted in a γ' fraction of 36,5 wt%, which is much higher than the 19,5 wt% predicted by JMatPro.

The amount of δ-phase present in the investigated specimen was precipitated during a pre-solution heat treatment step. This is generally recommended, if the as-forged material does not contain an adequate amount of δ-precipitates at the grain boundaries. The development of δ-phase will be studied in the following section.

Development of the δ-phase during heat treatment

It is the aim of the pre-solution heat treatment to homogeneously precipitate a large fraction of δ-phase at the grain boundaries. As this is favoured by rather slow precipitation kinetics, the optimum pre-solution temperature is well below the δ-solvus, e.g. in a range between 840 °C and 870 °C [13]. The beginning of the precipitation process for this temperature interval is shown in Figure 5. After 1 hr at 840 °C, small blocky plates have appeared at the grain boundaries (Figure

5a), a higher temperature of 870 °C leads to the formation of longer platelets (Figure 5b). Generally, δ-phase precipitates in a discontinuous manner, growing from the grain boundaries into the grain interior.

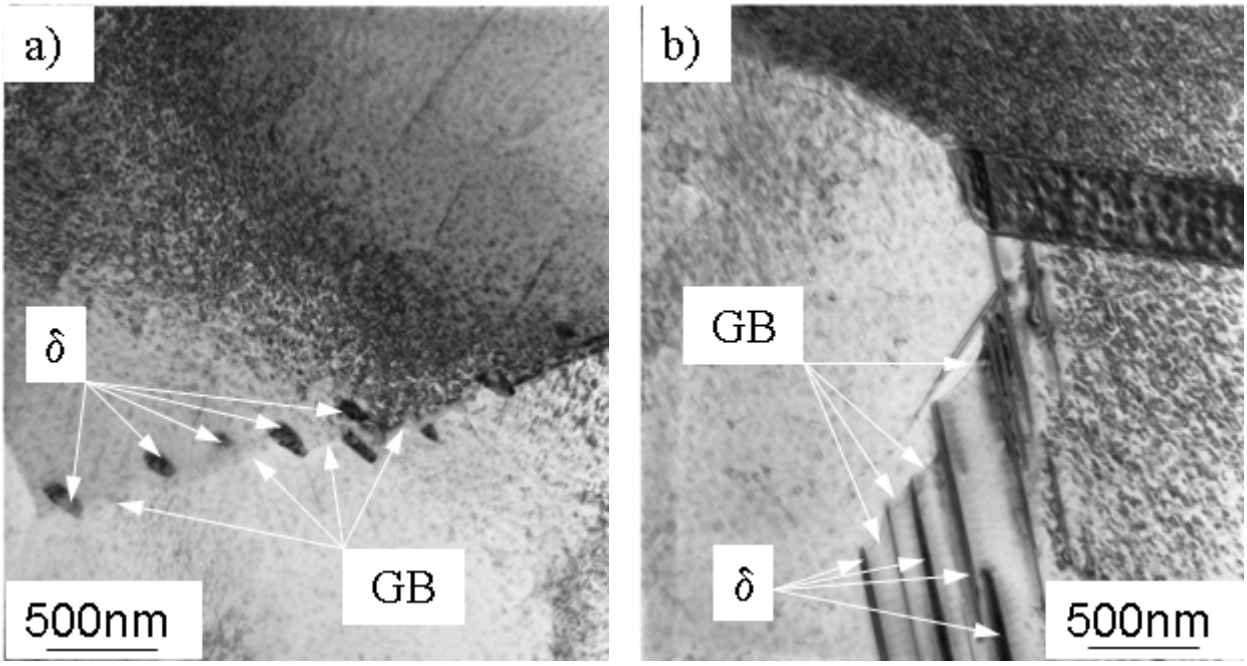

Figure 5: TEM micrographs showing the process of beginning discontinuous δ-precipitation: a) precipitation after 1 hr at 840 °C, b) precipitation after 1 hr at 870 °C. Typically, the precipitates grow from the grain boundary (GB) to the grain interior.

After pre-solution treatment, the resulting microstructure has a large amount of grain boundaries decorated with δ-phase. To preserve this microstructure, which is desirable with respect to grain boundary pinning and mechanical properties, the parameters for the following standard heat treatment steps, especially the solution temperature, need to be chosen carefully. While δ-precipitation continues at low solution temperatures around 950 °C, local dissolution of δ-phase might already take place at higher solution temperatures of around 980 °C.

Another obvious feature in Figure 5 is the parallel alignment of the δ-plates, indicating a fix crystallographic relationship with the Ni-matrix as known from 718, which will be further investigated below.

Composition of δ-phase

Figure 6a) shows a TEM micrograph of a colony of parallel δ-platelets. While γ′-particles are present in the regions outside this colony, the δ-platelets themselves are surrounded by a γ′-particle free region and also no γ′-particles are present between the δ-platelets. The fact that the γ′-particles are really dissolved between the δ-particles is evident from the SAD pattern in Figure 6b) which is recorded at the respective position between the δ-particles marked in Figure 6a). It shows the {110} diffraction pattern of the face centred cubic Ni-structure but the superlattice reflections typical for the ordered γ′-phase are missing. Figure 6c) shows the combined SAD pattern of the Ni-matrix and the δ-phase recorded at the position marked as c) in Figure 6a). In

addition to the reflections of Ni, which also appear in Figure 6b), now the diffraction pattern of the orthorhombic $D0_a$-structure of the δ-phase under [100] orientation is visible. That means that the δ-phase fulfils the same orientation relationship with the Ni-matrix as known and reported for 718, i.e. $[100]_\delta \| <110>_{\gamma/\gamma}$ and $(010)_\delta \| \{111\}_{\gamma/\gamma}$ [14].

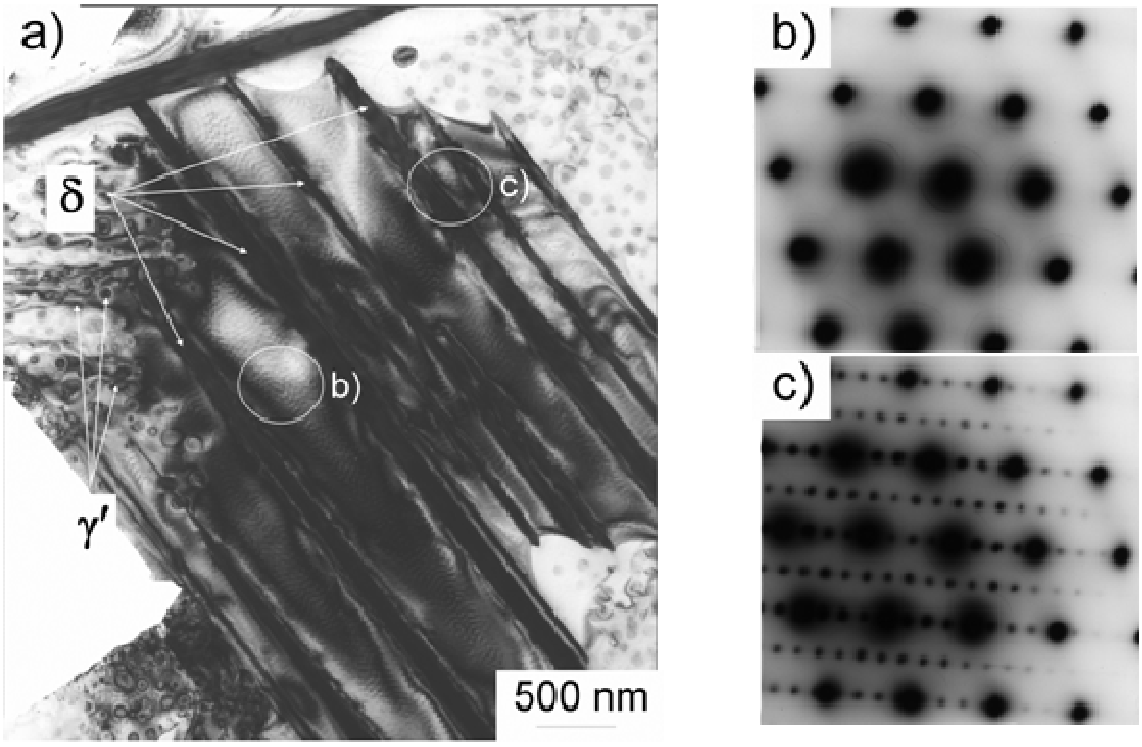

Figure 6: a) Colony of parallel δ-particles; b) diffraction pattern of an area between the δ phases; c) diffraction pattern of the δ particles combined with the underlying matrix; the locations where the diffraction patterns were recorded are marked in a); direction of incident beam is parallel to <1-10> of the Ni-matrix.

The fact that the δ-platelets are surrounded by a γ′-phase free zone is understandable from the chemical composition of the δ-phase. This was measured by EDX in the TEM and the results are given in Table 3. It is visible that the actual composition of the δ-phase present in 718Plus deviates from the stochiometry of the Ni_3Nb prototype δ-phase. While still large amounts of Ni and Nb are present, besides additional constituents with smaller concentrations as for example Cr, Fe and Co, especially the high content of Al in the above 9 % range is noteworthy. This means that typical γ′-building elements are enriched in the δ-phase. Thus, when δ-particles precipitate and grow, the surrounding alloy is depleted from Al, Nb and Ti and the local chemical composition in the vicinity of the growing δ-particles is changed to such an extent that the γ′-phase dissolves. The growing δ-particle consumes the γ′-particles in its direct vicinity.

Table 3: Composition of δ phase in 718Plus (at%).

Element	**Al**	**Ti**	**Cr**	**Fe**	**Co**	**Ni**	**Nb**	**Mo**	**W**
δ phase	9,12	3,42	4,40	2,86	6,88	61,1	11,5	0,55	0,28

Due to the chemical similarity between δ- and γ'-phase, a transformation mechanism from γ'- to δ-phase is possible. Evidence for this is visible from Figure 7. There, a TEM-micrograph is shown that was recorded under dark field conditions using the <001> superlattice reflection of the γ'-phase. Accordingly, the γ'-particles appear in bright contrast. While in the direct surrounding of the narrow δ-precipitates, arranged in parallel from the lower right to the upper left hand corner of the micrograph, no γ'-particles are found (in accordance with what is reported above), a bright rim is directly surrounding the δ-precipitates. As this rim is under bright contrast for an imaging condition using the superlattice reflection of the γ' phase it is assumed that this rim consists of γ' while the center of the platelet which shows no contrast is probably of the $D0_a$ δ-structure. It also appears, that some γ'-particles (marked by arrows) have grown together with this γ'-rim surrounding the δ-precipitate. This means, that the process of δ-phase precipitation can be described as a joining of γ'-precipitates building a γ'-platelet which in its interior transforms to the δ-crystal structure. Growth in width of this δ-phase probably happens by subsequently transforming the outer γ'-phase rim to δ-phase while γ'-building elements diffuse through the matrix to the γ' / δ-compound and build new layers of γ'-phase at the outer side of the γ'-rim.

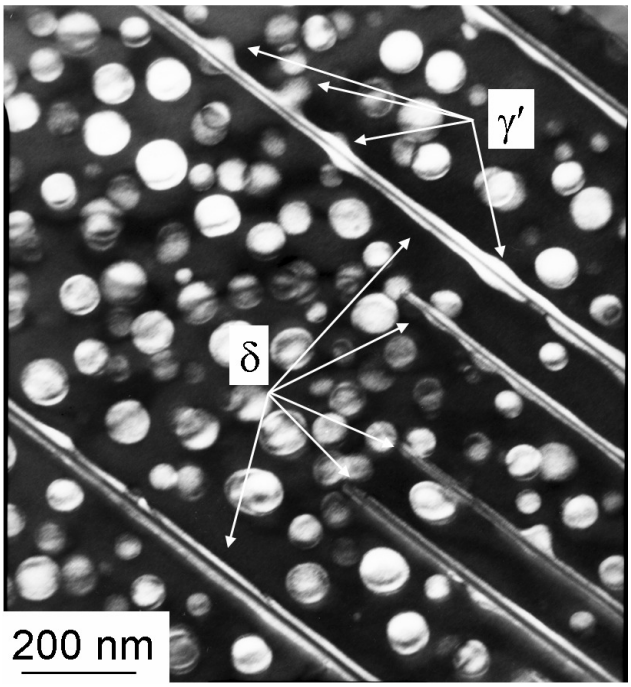

Figure 7: TEM dark field micrograph using the <001> superlattice reflection of the γ' phase showing γ' as bright ribbons at the edges of δ-phase. Specimen after pre-solution heat treatment at 840 °C for 16 hrs.

Consequently, δ-phase does not precipitate directly from the Ni-matrix, but is the product of a transformation mechanism from γ' to δ. In addition, growth of δ-precipitates can take place by this mechanism. Currently, more work is in progress to establish the long-term stability of 718Plus.

Detailed investigation of δ-phase and δ/ γ-interface

The identification of the δ-phase and its crystallographic orientation relationship with respect to the nickel γ-matrix is possible by means of evaluating selected area diffraction (SAD) patterns. Nevertheless, this neither gives information about the exact character of the δ / γ interface nor is it easily possible to exclude that not the orthorhombic δ-phase but a hexagonal Ni_3Nb-phase is present as claimed by Xie et al. [15]. So the interface region between a δ-phase precipitate and the neighboring γ-matrix was investigated by high resolution transmission electron microscopy (HRTEM). Figure 8a) shows in low magnification the δ-phase particle under investigation together with a neighboring grain. The specimen was oriented so that the δ-precipitate as well as the Ni-matrix in the neighboring grain had a certain crystallographic orientation parallel to the incident beam. This were the [100] orientation and the <110> orientation for the δ-phase and the Ni-matrix, respectively. This relationship is also known for 718 [14].
Figure 8b) shows the interface between the δ-phase and the Ni-matrix under higher magnification. In the Ni-matrix the ABC stacking order of a face centered cubic phase is easily discernible. The direction of the {111} closed packed planes is marked in the micrograph. These {111} planes are parallel to the interface between the δ-precipitate and the Ni-matrix, which appears to be flat. To identify the crystallographic plane of the δ-phase, which is parallel to the δ / γ-interface, the experimental HRTEM picture of the δ-precipitate is compared with a simulated HRTEM image.

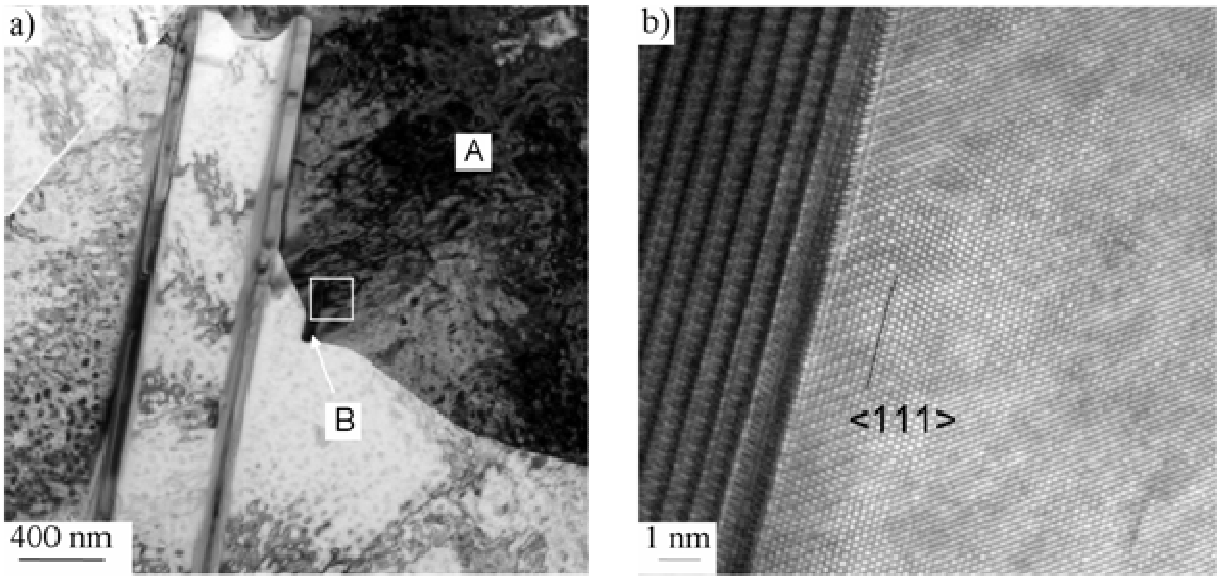

Figure 8: a) overview of the positions for HRTEM investigations; one grain with orientation parallel to <110> (A) and δ phase particle (B) at an adjacent grain boundary; b) interface between the δ particle and the neighbouring γ grain showing the flat δ / γ interface parallel to a set of {111} planes in the matrix.

In Figure 9a) a HRTEM micrograph of the δ-phase is shown with a simulated HRTEM picture as inset to demonstrate that the experimentally recorded picture is in accordance with the expected intensity distribution for an orthorhombic $D0_a$ structure under [100] orientation which is the lattice cell for the δ-phase. In Figure 9b) a larger portion of this simulated image is shown with the positions of the Ni- and Nb-atoms as overlay. It is visible that the (010) crystallographic planes of the δ-phase are parallel to the δ / γ-interface (note that image in Figure 9b) is rotated

relative to Figure 8b). Due to the good matching of the experimental HRTEM picture of the δ-phase with the simulated HRTEM image of a $D0_a$ structure it is also evident, that the particle under investigation is really a δ-phase particle and not a hexagonal $Ni_3Nb_{0.5}Al_{0.5}$-phase of the kind found by Xie et al. So while it is not possible to fully exclude that small fractions of this hexagonal phase are present in the 718Plus specimens under investigation here from HRTEM investigations and especially from diffraction analysis performed on a large number of particles it can be stated that nearly all if not all precipitates are δ-phase. The absence of the hexagonal phase in our specimens in discrepancy to the results of Xie et al. may stem from a different heat treatment.

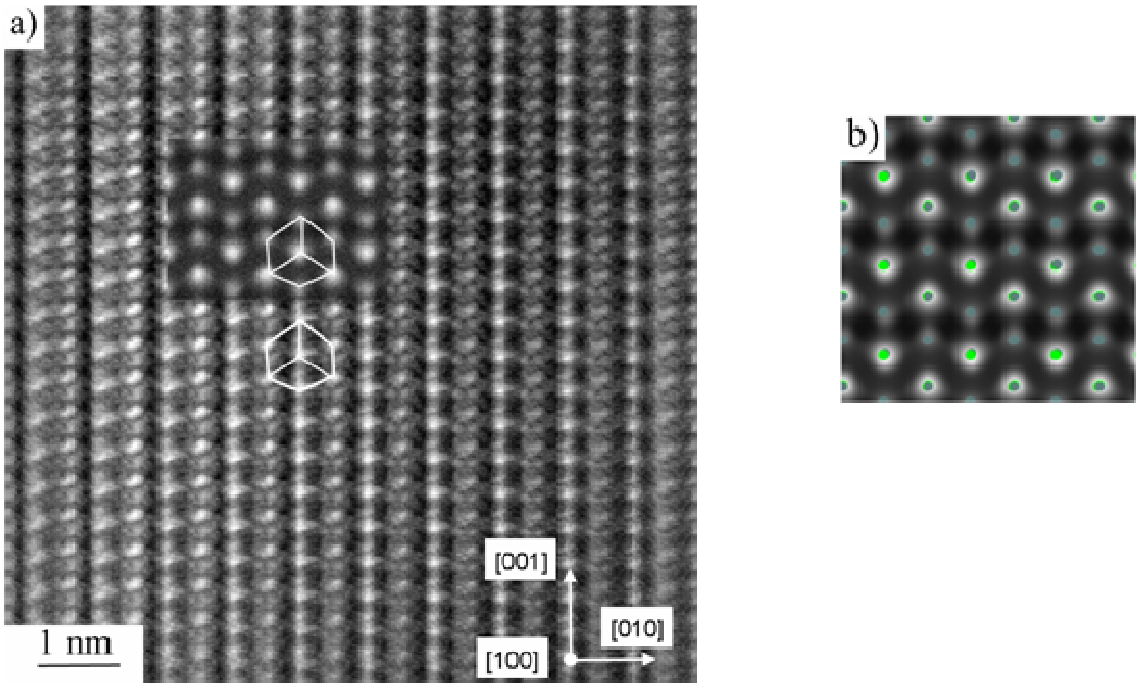

Figure 9: a) HRTEM micrograph of the δ phase recorded along the [100] direction (image slightly rotated relative to Figure 8b), inset showing a simulated HRTEM picture, lines in simulated and experimental picture show coincidence of lattices; b) higher magnification of the simulated HRTEM picture with respective atomic positions in color (bright green: Nb, dark green: Ni, foil thickness: 9.2 nm, defocus: -18.5 nm).

Possibility of γ'' phase in 718Plus

While the design of 718Plus aimed on hardening the alloy with γ′ phase it may well be that a certain amount of γ″-phase, which is responsible for hardening of alloy 718, is also present in 718Plus. In JMatPro calculations with suppressed δ-phase, γ'' with a solvus of 913 °C occurs instead of δ. To investigate this point, the globular precipitates present in the different heat treatment states of the alloy under investigation ranging from solution heat treated to different states of ageing at 788 °C and 704 °C, respectively, were characterised by SAD. From the diffraction patterns it is evident that the globular precipitate phase in the grain interior is predominantly the γ′-phase. An example of such a diffraction pattern recorded along the <001> zone axis of the Ni-matrix is shown in Figure 10a). The different diffraction spots are indexed in

Figure 10a) and besides the {200} and {220} reflections of the fcc Ni-matrix also the {100} and {110} superlattice reflections of the ordered $L1_2$ structure of the γ′-phase are clearly visible.

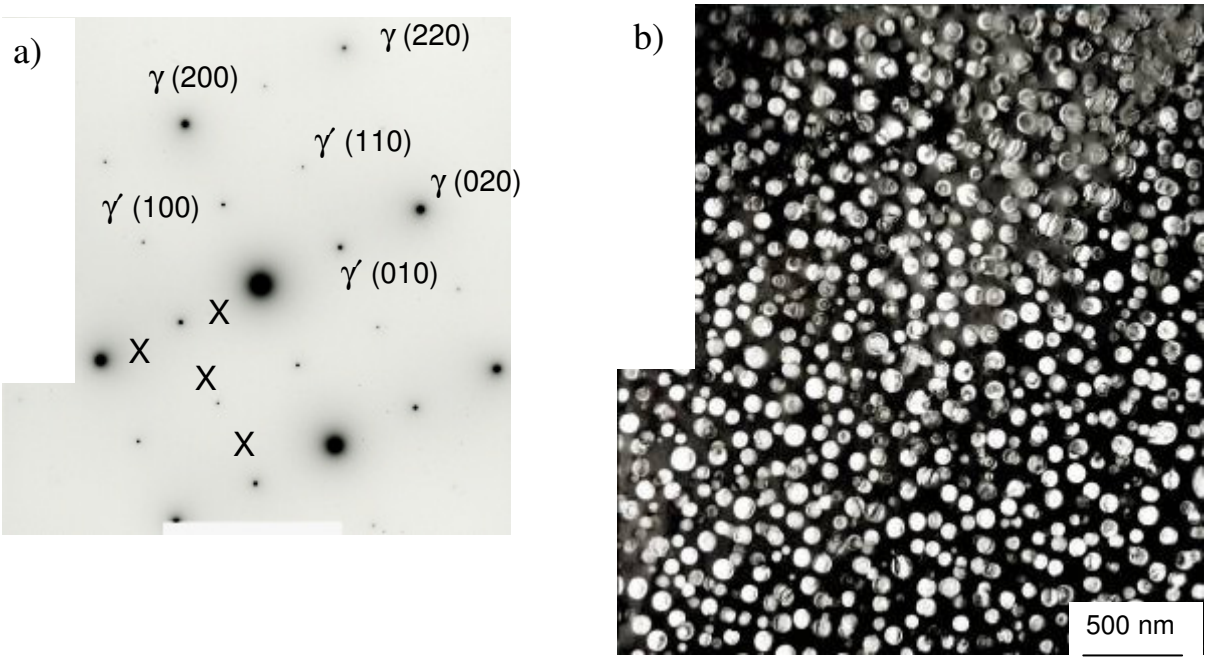

Figure 10: a) Diffraction pattern recorded with incident beam parallel to the <001> crystallographic orientation showing reflections of the Ni-matrix (200, 220, 020, etc.) and superlattice reflections of the ordered γ′-precipitate phase (100, 110, 010); no reflections indicating the presence of the γ″-phase are visible (respective positions marked with X); b) dark field TEM micrograph of the γ′-precipitate phase using the (100) superlattice reflection; specimen annealed for 16 hrs at 870 °C.

From the dark field TEM micrograph shown in Figure 10b), which was recorded using the {100} superlattice reflection of the γ′-phase, it can be seen that the globular precipitates are γ′-particles. If γ″-phase was present it should show distinct reflections at the positions marked by crosses in Figure 10a). Neither in the diffraction pattern shown here nor in a number of other diffraction patterns taken in specimens of different heat treatment conditions, any evidence of the γ″-phase could be found. As other authors [16] report small amounts of γ″-phase to be present in 718Plus, we suppose that the absence of γ″-phase in the specimens under investigation here stems from the chosen heat treatment conditions.

Conclusions

In the present study, phase stability and microstructure evolution of 718Plus during heat treatment have been characterised by TEM in particular.

- The two major phases were found to be γ′- and δ-phase.
- After ageing heat treatment, γ' precipitates show a monomodal size distribution within the matrix. Apparently, γ' coarsening is rather slow and proportional to $t^{1/3}$. The γ' weight fraction was determined to be 36,6 %, which is higher than the value predicted by JMatPro. Al, Ti and Nb mainly partition to the γ' phase.

- Colonies of parallel δ-phase platelets precipitate discontinuously starting from the grain boundaries. Similar to γ', Al, Nb and Ti are the main constituents of δ-phase. Therefore, γ' free zones frequently surround δ-precipitates.
- By analysing selected area diffraction patterns from a large number of particles it could be shown that nearly no γ''-phase is present in the alloy.
- The orientation relationship between the δ-phase and the γ/γ'-phase is $[100]_{\delta} \| <110>_{\gamma/\gamma}$ and $(010)_{\delta} \| \{111\}_{\gamma/\gamma}$ as known from 718. The interfaces between the δ- and surrounding γ/γ'-phase are flat and parallel to the {111} plane of the γ/γ'-phase and accordingly the (010) plane of the δ-phase.

Acknowledgements

The authors would like to thank Rolls-Royce for the permission to publish this work. This research has been funded by the German Government under the "Luftfahrtforschungsprogramm LuFoIV" framework programme.

References

1 Loria, E.A. (Ed.), Superalloys 718, 625, 706 and Various Derivatives, 2005, TMS, Warrendale, PA, USA

2 Cao, W.D., Kennedy, R.L., Superalloys 2004, TMS, Warrendale, PA, USA, 91-99

3 Cao, W., Kennedy, R.L., United States Patent No. US 7.156.932 B2, USA, 2007

4 Ott, E.A., Groh, J., Sizek, H., Superalloys 718, 625, 706 and Various Derivatives 2005, TMS, Warrendale, PA, USA, 35-45

5 Saunders, N., Ni-DATA version 7, Thermotech Ltd., The Surrey Research Park, Guildford, Surrey, UK

6 Cao, W.D., Superalloys 718, 625, 706 and Various Derivatives, 2005, TMS, Warrendale, PA, USA, 165-177

7 Stotter, C., Sommitsch, C., Wagner, J., Leitner, H., Letofsky-Pabst, I., Stockinger, M., International Journal of Materials Research 99 (4), 2008, 376-380

8 Hardy, M.C., Zirbel, B., Shen, G., Shankar, R., Superalloys 2004, TMS, Warrendale, PA, USA, 83-90

9 McDevitt, E.T., Bentley, J., Materials for High Temperature Applications: Next Generation Superalloys and Beyond, TMS, San Francisco, FL, USA, 2009, 289-296

10 Zickler, G.A., Schnitzer, R., Radis, R., Hochfellner, R., Schweins, R., Stockinger, M., Leitner, H., Materials Science and Engineering A 523, 2009, 295-303

11 Tamarin Y., Protective Coatings for Turbine Blades, 2002, ASM International, OH, USA

12 Blavette, D. Caron, P., Khan, T., Superalloys 1988, TMS, Warrendale, PA, USA, 305-314

13 Dempster, I., Cao, W.D., Kennedy, R., Bond, B., Aurrecoechea, J., Lipschutz, M., Superalloys 718, 625, 706 and Various Derivatives 2005, TMS, Warrendale, PA, USA, 155-164

14 Rong, Y., Chen, S., Hu, G., Gao, M., Wei, R., Metallurgical and Materials Transactions A 30, 1999, 2297-2303

15 Xie, X., Xu, C., Wang, G., Dong, J., Cao, W.D., Kennedy, R., Superalloys 718, 625, 706 and Various Derivatives 2005, TMS, Warrendale, PA, USA, 193-202

16 Unocic, K.A., Hayes, R.W., Daehn, G.S., Metallurgical and Materials Transactions A 41, 2010, 409-420